Appendix A. Supplementary information to: "Cyclostratigraphy and eccentricity tuning of the early Oligocene through early Miocene (30.1–17.1 Ma): *Cibicides mundulus* stable oxygen and carbon isotope records from Walvis Ridge Site 1264"

Liebrand et al.

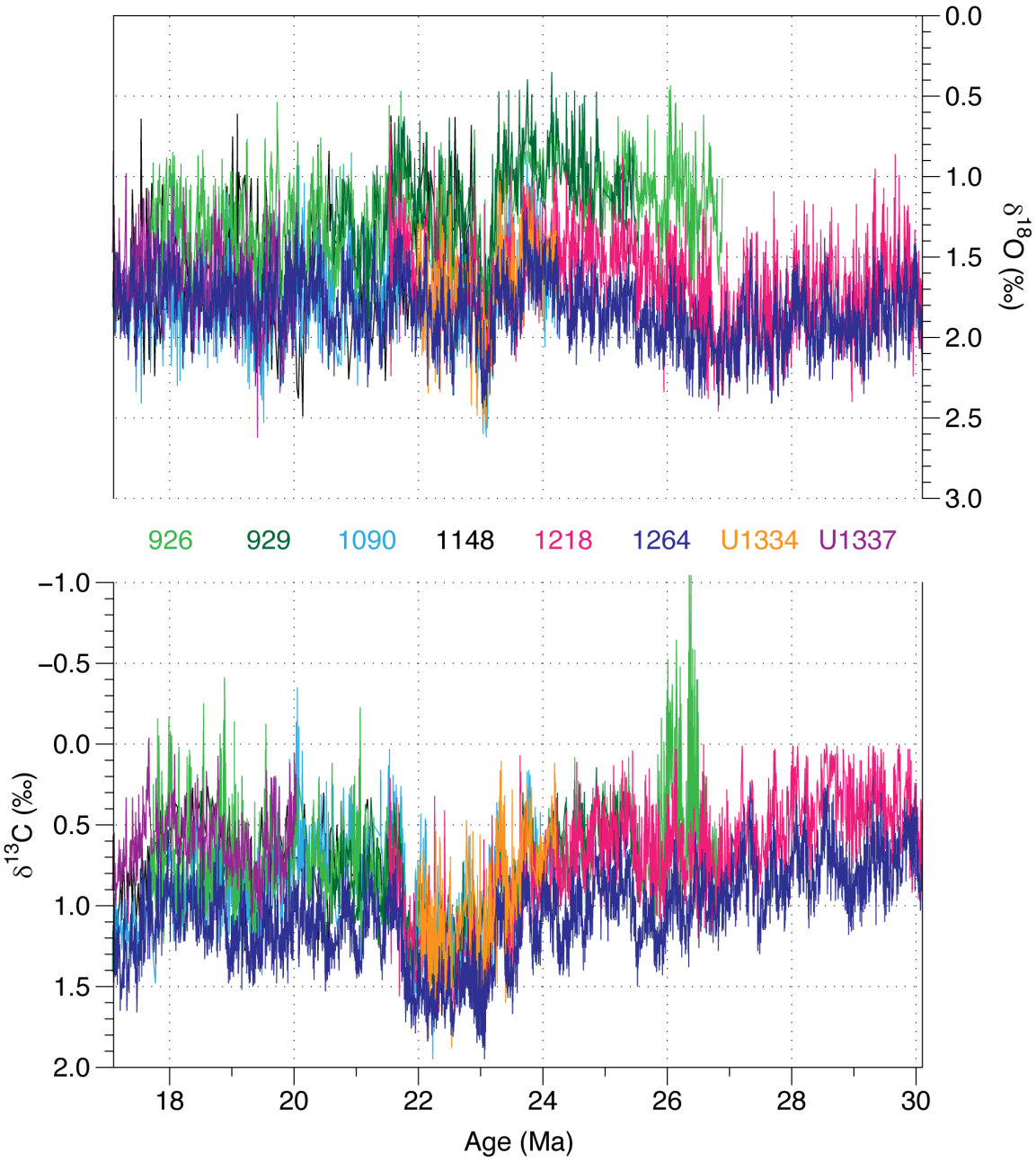

Fig. S1. Comparison of high resolution Oligo-Miocene benthic stable isotope stratigraphies. Benthic foraminiferal records from ODP Sites 926 & 929 (Flower et al., 1997; Pälike et al., 2006a; Paul et al., 2000; Zachos et al., 1997; Zachos et al., 2001), 1090 (Billups et al., 2004), 1146 (Tian et al., 2008), 1218 (Coxall et al., 2005; Lear et al., 2004; Pälike et al., 2006b; Tripati et al., 2006; Wade and Pälike, 2004), 1264 (this study, (Liebrand et al., 2011)), and from IODP Sites U1334 (Beddow et al., 2016) and U1337 (Holbourn et al., 2015).

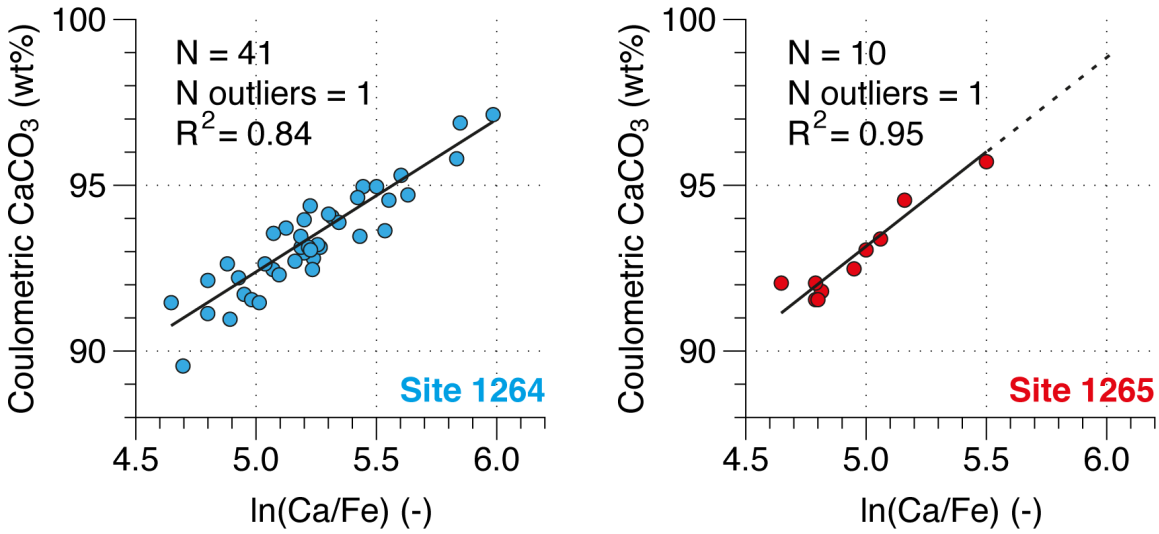

Fig. S2. Estimating $CaCO_3$ content. XRF data (ln(Ca/Fe)) from ODP Sites 1264 and 1265 (Fig. 1 of main document) are calibrated to shipboard coulometric $CaCO_3$ measurements (Zachos et al., 2004) to obtain $CaCO_3$ est. records.

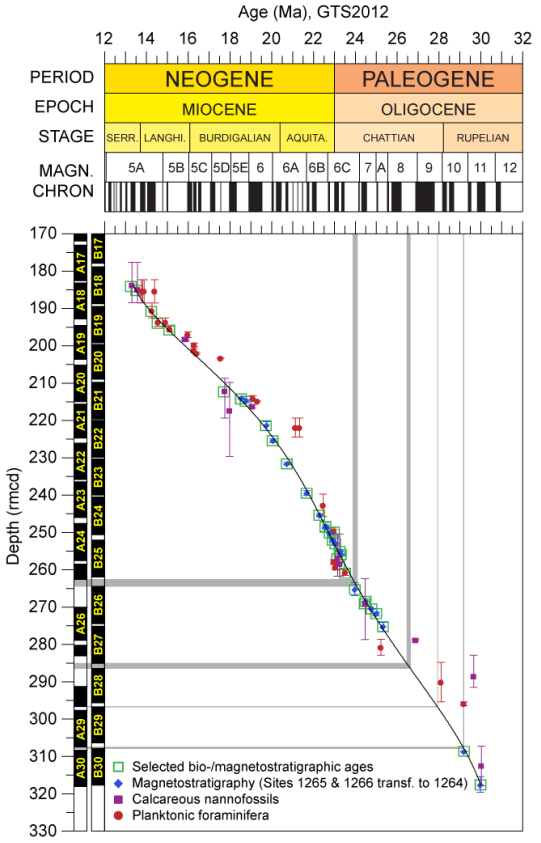

Fig. S3. Initial age-model for ODP Site 1264. A polynomial function describes the initial depth-age relation used to aid assessing the duration of the main oscillations in the depth-domain. Shipboard biostratigraphic and magnetostratigraphic data were used to construct the initial age-model (Bowles, 2006; Zachos et al., 2004).

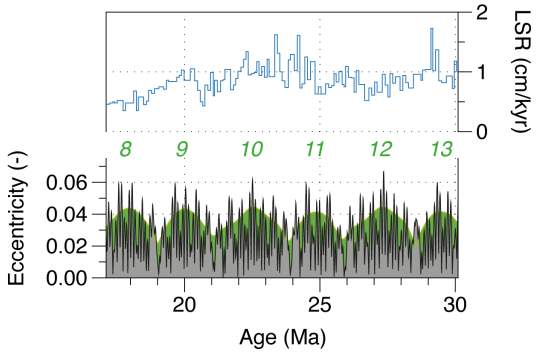

Fig. S4. Linear sedimentation rates (LSR) at ODP Site 1264. LSRs are calculated between tuning tie-points (i.e. ~110-kyr eccentricity minima (Laskar et al., 2011)) and vary between 1.7 and 0.4 cm/kyr, or between 17 and 4 m/Myr.

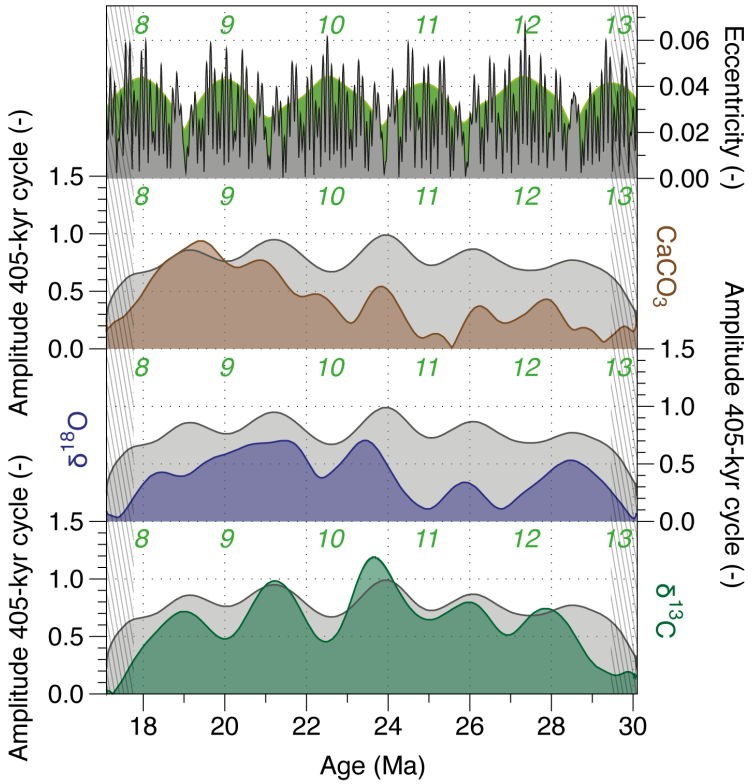

Fig. S5. ~2.4-Myr-eccentricity amplitude modulation of the 405-kyr-eccentricity cycle. The top panel depicts the La2011_ecc3L eccentricity solution (grey) (Laskar et al., 2011) and the amplitude modulation of its ~2.4-Myr component (green). The bottom three panels show the Hilbert-transforms of normalised, detrended, and Gaussian filtered data (coloured) and eccentricity (grey). The ~2.4-Myr eccentricity cycle numbers are given in green.

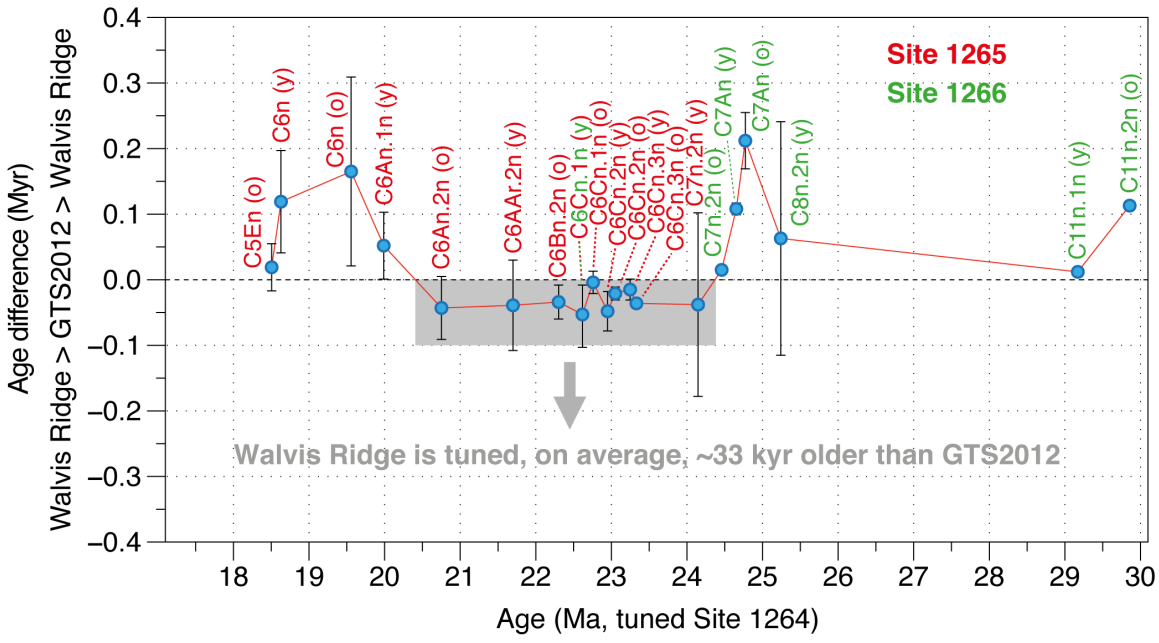

Fig. S6. Palaeomagnetic data from Walvis Ridge. Age differences between the tuned magnetostratigraphies from ODP Sites 1265 and 1266 and the GTS2012 are depicted. This figure is a visual representation of Table 1 in the main document.

1. BIOSTRATIGRAPHY

1.1. Rationale and methods

Comparison of the shipboard biostratigraphic results from Site 1264 (Zachos et al., 2004) with published data from Sites 926 and 929 (Pälike et al., 2006a; Shackleton et al., 2000) suggested that the ranges of calcareous nannofossil *Sphenolithus delphix* did not (fully) overlap. We wanted to test the robustness of this apparent and unexpected diachrony because *S. delphix* is one of the key OMT marker species that has generally proved to be a reliable datum (Raffi, 1999). Therefore, we have generated records of *Sphenolithus* counts (N/mm^2) based on selected samples across the OMT interval, which record the abundances of *S. delphix*, and other OMT marker species, namely *Sphenolithus calyculus*, *Sphenolithus capricornutus* and *Sphenolithus disbelemnos* in detail. At Chieti University, smear-slides of bulk sediment were made using standard preparation techniques, and were analysed with a polarizing microscope at 1250× magnification. In addition to the quantitative Sphenolith stratigraphies, the abundance of *Triquetrorhabdulus carinatus* was qualitatively evaluated.

1.2. Results

The preservation of calcareous nannofossils at Site 1264 is moderately affected by dissolution. Despite this suboptimal signal we have been able to evaluate the relative abundances and constrain the ranges of those *Sphenolithus* species related to the OMT (Raffi, 1999). *S. delphix* and *S. capricornutus* show the typical variability in their distribution ranges, comparable to other locations. During a $\delta^{18}O$ maximum, about 405 kyr prior to the OMT (at ~260 armcd, ~23.7 Ma, during 405-kyr eccentricity Cycle 59, Supp. Fig. S7), the lowermost occurrence of *S. delphix* (peaking at 7 per mm^2) is concomitant with more abundant *S. calyculus* specimens (22 per mm^2). *S. delphix* re-enters (peak 19 per mm^2) the stratigraphic record contemporaneously with the onset of the transient glaciation across the OMT (between 255–254 armcd, 23.2–23.1 Ma, 405-kyr eccentricity Cycle 58, Supp. Fig. S7). At this time, also *S. capricornutus* shows a peak in abundance (57 per mm^2). In the interval below the main peak in *S. capricornutus* (~256 armcd, ~23.3 Ma), rare specimens of *S. disbelemnos* are recorded (8 per mm^2). The gradual decrease in the abundance of *T. carinatus* across the Oligocene-Miocene Transition from Site 1264 is characteristic of the younger part of its distribution range, and is in agreement with observations from other marine locations (Backman et al., 2012).

1.3 New age calibrations for selected Oligo-Miocene nannofossil markers

These new results show that the apparent diachrony between the shipboard range of *S. delphix* at Site 1264 with the one from Site 926 is no longer present. However, the updated range of *S. delphix* at Site 1264, presented here, is twice as long compared to those of Sites 926 and 1218. A similar, longer distribution range for *S. delphix* has also been observed in the North Atlantic at Site U1405 (Agnini, 2016; Norris et al., 2012). Recent age-calibration of *S. delphix* at Site 1218 indicated that it ranged from 23.38 to 23.06 Ma (Backman et al., 2012). The longer range of *S. delphix* found at Site 1264 has age limits of 23.73 to 23.11 Ma, thereby extending the bottom age by ~350 kyr. The restricted occurrence of *S. disbelemnos* at Site 1264 precedes the known earliest occurrence of this biostratigraphic marker, which is calibrated elsewhere at 22.41 Ma (Backman et al., 2012), by ~980 kyr. We find an earliest occurrence of *S. disbelemnos* at 23.39 Ma.

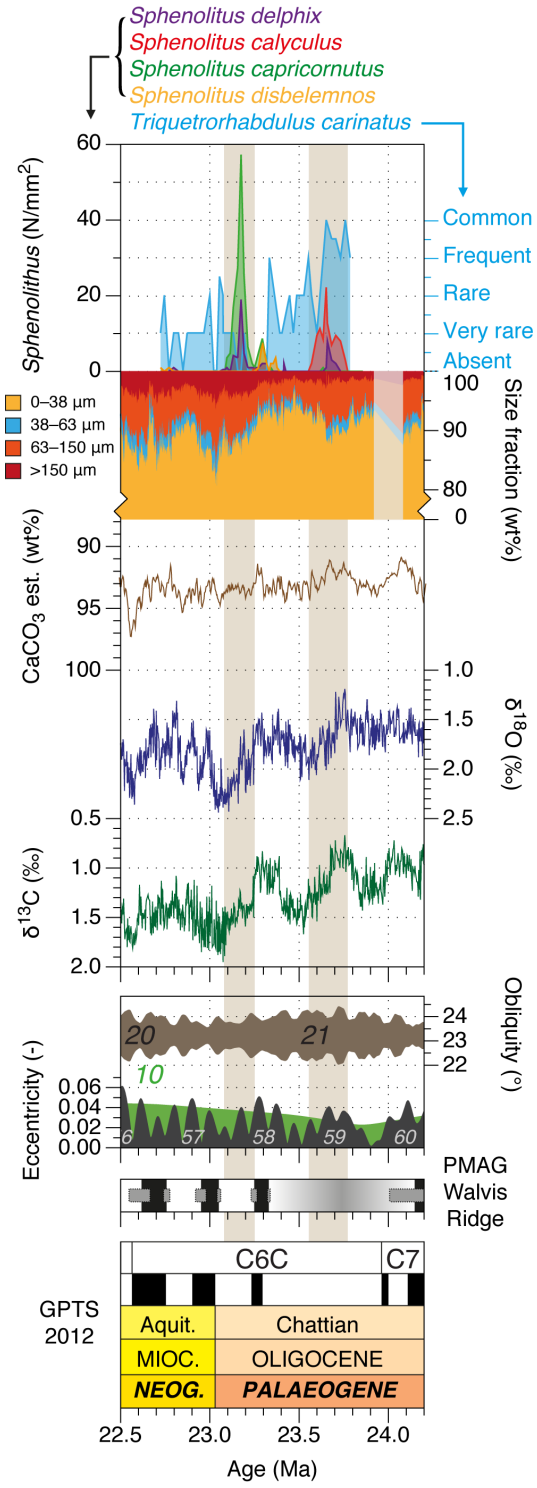

Fig. S7. Calcareous nannofossil stratigraphy across the Oligocene-Miocene Transition. Quantitative and qualitative nannofossil abundances are compared to proxy records and the GTS2012 (Hilgen et al., 2012; Vandenberghe et al., 2012). See Fig. 4 in the main document for a further explanation.

References

Agnini, C., 2016. pers. comm.

Backman, J., Raffi, I., Rio, D., Fornaciari, E., Pälike, H., 2012. Biozonation and biochronology of Miocene through Pleistocene calcareous nannofossils from low and middle latitudes. Newsletters on Stratigraphy 45, 221 - 244.

Beddow, H.M., Liebrand, D., Sluijs, A., Wade, B.S., Lourens, L.J., 2016. Global change across the Oligo-Miocene Transition: High-resolution stable isotope records from IODP Site U1334 (equatorial Pacific Ocean). Paleoceanography 31, 81–97

Billups, K., Pälike, H., Channell, J.E.T., Zachos, J., Shackleton, N.J., 2004. Astronomic calibration of the late Oligocene through early Miocene geomagnetic polarity time scale. Earth and Planetary Science Letters 224, 33-44.

Bowles, J., 2006. Data report: revised magnetostratigraphy and magnetic mineralogy of sediments from Walvis Ridge, Leg 208, in: Kroon, D., Zachos, J.C., Richter, C. (Eds.), Proc. ODP, Sci. Results, 208. Ocean Drilling Program, College Station, TX.

Coxall, H.K., Wilson, P.A., Pälike, H., Lear, C.H., Backman, J., 2005. Rapid stepwise onset of Antarctic glaciation and deeper calcite compensation in the Pacific Ocean. Nature 433, 53-57.

Flower, B.P., Zachos, J.C., Martin, E., 1997. Latest Oligocene through early Miocene isotopic stratigraphy and deep-water paleoceanography of the Western Equatorial Atlantic: Sites 926 and 929, in: Shackleton, N.J., Curry, W.B., Richter, C., Bralower, T.J. (Eds.), Proceedings of the Ocean Drilling Program, Scientific Results., pp. 451 - 461.

Hilgen, F.J., Lourens, L.J., van Dam, J.A., 2012. The Neogene period. In: Gradstein, F.M., Ogg, J.G., Schmitz, M., Ogg, G.M. (Eds.), The Geologic Time Scale 2012. Elsevier.

Holbourn, A., Kuhnt, W., Kochhann, K.G.D., Andersen, N., Meier, K.J.S., 2015. Global perturbation of the carbon cycle at the onset of the Miocene Climatic Optimum. Geology.

Laskar, J., Gastineau, M., Delisle, J.-B., Farrés, A., Fienga, A., 2011. Strong chaos induced by close encounters with Ceres and Vesta. Astronomy and Astrophysics 532, 1-4.

Lear, C.H., Rosenthal, Y., Coxall, H.K., Wilson, P.A., 2004. Late Eocene to early Miocene ice sheet dynamics and the global carbon cycle. Paleoceanography 19.

Liebrand, D., Lourens, L.J., Hodell, D.A., De Boer, B., Van de Wal, R.S.W., Pälike, H., 2011. Antarctic ice sheet and oceanographic response to eccentricity forcing during the early Miocene. Climate of the Past 7, 869-880.

Norris, R.D., Wilson, P.A., Blum, P., Expedition_342_Scientists, 2012. Paleogene Newfoundland Sediment Drifts, IODP Prel. Rept. Inegrated Ocean Drilling Prgram.

Pälike, H., Frazier, J., Zachos, J.C., 2006a. Extended orbitally forced palaeoclimatic records from the equatorial Atlantic Ceara Rise. Quaternary Science Reviews 25, 3138-3149.

Pälike, H., Norris, R.D., Herrle, J.O., Wilson, P.A., Coxall, H.K., Lear, C.H., Shackleton, N.J., Tripati, A.K., Wade, B.S., 2006b. The heartbeat of the Oligocene climate system. Science 314, 1894-1898.

Paul, H.A., Zachos, J.C., Flower, B.P., Tripati, A., 2000. Orbitally induced climate and geochemical variability across the Oligocene/Miocene boundary. Paleoceanography 15, 471-485.

Raffi, I., 1999. Precision and accuracy of nannofossil biostratigraphic correlation. Phil. Trans. R. Soc. Lond. 357.

Shackleton, N.J., Hall, M.A., Raffi, I., Tauxe, L., Zachos, J.C., 2000. Astronomical calibration age for the Oligocene-Miocene boundary. Geology 28, 447-450.

Tian, J., Zhao, Q., Wang, P., Li, Q., Cheng, X., 2008. Astronomically modulated Neogene sediment records from the South China Sea. Paleoceanography 23.

Tripati, A., Elderfield, H., Booth, L., Zachos, J., Ferretti, P., 2006. Data Report: High-Resolution Benthic Foraminiferal Stable Isotope Stratigraphy across the Oligocene/Miocene Boundary at Site 1218, in: Wilson, P.A., Lyle, M., Firth, J.V. (Eds.), Proceedings of the Ocean Drilling Program, Scientific Results. Ocean Drilling Program.

Vandenberghe, N., Hilgen, F.J., Speijer, 2012. The Paleogene period. In: Gradstein, F.M., Ogg, J.G., Schmitz, M., Ogg, G.M. (Eds.), The Geologic Time Scale 2012. Elsevier.

Wade, B.S., Pälike, H., 2004. Oligocene climate dynamics. Paleoceanography 19.

Zachos, J.C., Flower, B.P., Paul, H.A., 1997. Orbitally paced climate oscillations across the Oligocene/Miocene boundary. Nature 388, 567-570.

Zachos, J.C., Kroon, D., Blum, P., Bowles, J., Gaillot, P., Hasegawa, T., Hathorne, E.C., Hodell, D.A., Kelly, D.C., Jung, J.-H., Keller, S.M., Lee, Y.S., Leuschner, D.C., Liu, H., Lohmann, K.C., Lourens, L.J., Monechi, S., Nicolo, M., Raffi, I., Riesselman, C., Röhl, U., Schellenberg, S.A., Schmidt, D., Sluijs, A., Thomas, D., Thomas, E., Vallius, H., 2004. Initial Reports: Leg 208, Proceedings of the Ocean Drilling Program. Ocean Drilling Program.

Zachos, J.C., Shackleton, N.J., Revenaugh, J.S., Palike, H., Flower, B.P., 2001. Climate response to orbital forcing across the Oligocene-Miocene boundary. Science 292, 274-278.